Numerical Methods in Civil Engineering, 8-2 (2023) 56-69

Numerical Methods in Civil Engineering

Journal Homepage: https://nmce.kntu.ac.ir/

Axial bearing capacity of helical piles in moist and saturated conditions using frustum confining vessel (FCV)

Ali Jassim *, Navid Ganjian **, Abolfazl Eslami ***

ARTICLE INFO

RESEARCH PAPER

Article history:
Received:
June 2022
Revised:
November 2022
Accepted:
December 2022

Keywords:
Helical Pile,
Axial Bearing Capacity,
Physical Modeling,
FCV Apparatus,
Anzali Sand

Abstract:

Due to the increasing demand in construction and use of different types of piles on the one hand and the high cost of conducting large-scale tests on different types of piles, on the other hand, new methods have been proposed to study the behavior of different types of piles. Physical modeling provides the researcher the capability of studying model piles in the scaled environment at low costs. Among the different methods of physical modeling, the use of frustum confining vessels (FCV) has gained attraction in recent years. FCV is a cone-shaped vessel that can produce a stress distribution similar to the idealized linear stress distribution in depth. Helical piles are common types of deep foundations which were first used about 200 years ago. Helical Apiles are driven to the soil by applying a torque to the end of piles in the presence of vertical loads. Their quick and noise-free installation method, the minimal disturbance during the installation, and environmental compatibility make them popular for working in urban areas. In this research, using the finite element method, the optimal dimensions of FCV apparatus were selected, and the FCV apparatus with optimal dimensions were constructed. A total of 18 compression tests were performed on Anzali sand in different relative densities and moisture contents, using single-helix and three-helices piles. Results indicate that increasing the number of helices and relative density of soil increases the pile and sand contact and causes higher bearing capacity for helical piles. Soil saturation, on the other hand, significantly reduces the ultimate strength.

1. Introduction

Over the past few decades, the increasing demand from oil and gas industries for the construction of facilities nearshore and offshore yielded to an increasing attraction to the deep foundations, i.e., piles. The foundations of many structures, whether on the land such as high-rise buildings and chimneys or marine structures such as wind turbines and towers are subjected to tension and compression loads[1, 2]; therefore, the study of the bearing capacity of such foundations attracted attention in the recent decades. Many research has been conducted on the numerical and experimental ultimate bearing capacity of piles[1-14].

** PhD Candidate, Department of Civil Engineering, Science and Research Branch, Islamic Azad University, Tehran, Iran.*
*** Corresponding author: Assistant Professor, Department of Civil Engineering, Science and Research Branch, Islamic Azad University, Tehran, Iran.*
**** Professor, Department of Civil and Environment Engineering, Amirkabir University, Tehran, Iran.*

A helical pile is a circular pile with a blade. It is an old type of pile that has recently become attractive due to its quick and silent installation and minimal disturbances during installation [9, 10]. Helical piles installation is carried out by applying torque at the end of the pile in the presence of vertical pressure [9]. The first usage of helical piles was as anchors for electrical towers, subjected to uplift force [10].

Physical modeling has been recognized as a beneficial tool for studying pile behavior. This is an important and sophisticated subject in the geotechnical field, that allows one to carry out many tests that are not expensive compared to field programs and offers the possibility of studying theoretical and practical viewpoints. Each apparatus used in physical modeling has its own advantages and disadvantages. Amongst the different physical modeling methods, Frustum Confining Vessel has gained increasing attraction in recent years due to its simplicity and the realistic stress distribution generation in depth. FCV apparatus is a truncated cone-shaped

https://doi.org/10.61186/NMCE.2022.438

vessel that was first introduced by Horvath and Stole at Mc.Master University in 1996 [15]. FCV can convert the applied uniform base pressure to horizontal and vertical components. By converting the applied pressure to two perpendicular components, FCV can produce a near-linear stress gradient for vertical and horizontal stress [15]. FCV benefits from the advantages of both Centrifuge and Calibration chambers and is capable of mimicking the stress distribution condition of in-situ soil [16].

As mentioned, the first FCV apparatus was introduced by Horvath and Stole at Mc.Master University in 1996. The next FCV devices were constructed at South Florida (1999), Amirkabir University of Technology (2012)[13], and Isfahan University of Technology (2019) [17]. The most recently constructed FCV apparatus was designed and fabricated by the authors at Baran Khak va Pey Company, Tehran, Iran. It has the largest top diameter amongst the existing FCV apparatus worldwide, providing the authors an invaluable tool for investigating the lateral and axial behavior of piles and the capability of testing piles with larger diameters (i.e., helical piles with larger helix diameters). The larger top diameter also minimizes errors related to scale effects and boundary effects. Additionally, the newly constructed FCV device is capable of testing model piles in saturated and near-saturated soil conditions (Similar to nearshore and offshore soil conditions). The readers are encouraged to refer to another paper by the authors[18] for more information regarding the newly constructed FCV apparatus, i.e., its dimensions, instrumentations, and saturating process.

Many research has been carried out using FCV to study the different aspects of piles behavior. Zare and Eslami [13] studied the key features of FCV-AUT in terms of stress distribution in depth and performed a couple of axial loading tests on three driven steel piles. Results indicated a close agreement between the numerically predicted bearing capacity, using the ESA method, and the experimentally measured bearing capacity.

Karimi and Eslami [19], Khazaei and Eslami [20], and Karimi et al. [21] investigated the effects of soil improvement techniques, such as soil densification and post-grouting, to compensate for the disturbances that occurred during pile installation. Different types of piles, such as open-ended piles, close-ended piles, H steel piles, and helical piles, have been scrutinized. They concluded that increasing the soil-pile interaction by post-grouting of the base and sides of the pile, as well as soil compaction yields, to an increase in soil-bearing capacity.

Khazaei and Eslami [20] investigated the geotechnical behavior of different types of piles, including helical piles, with the aid of FCV-AUT. They concluded that a helical pile with two helices shows a performance equal to a steel pile with a shaft diameter equivalent to the helix diameter of the screw pile. In other words, using helical piles can yield approximately a 50% decrease in cost of materials.

Zarrabi and Eslami [22] scrutinized the construction effects on the performance of piles, using physical modeling in FCV-AUT.

Askari Fateh, Eslami, and Fahimifar [23] studied the failure mechanism of three helical piles made up of hollow galvanized iron pipes with one, two, and three helices. The experimental results were verified using two static analysis methods, CFEM (2006) and Vessic (1997). They concluded that the CFEM formulation has shown a more realistic prediction of the ultimate bearing capacity. They also affirmed the conclusion made by the other researchers that depending on the helix spacing ratio, individual or cylindrical failure mechanisms may occur (Perko [24]). For helical piles in sand, the transition from cylindrical failure to individual bearing behavior occurs at a helix spacing ratio (S/D) of about three (Lutenegger [25]).

FCV apparatus provides a scaled environment for testing both conventional and newly developed piles. Shojaei et al. [26] performed a feasibility study on the use of a new type of self-expanded piles aiming to reduce the harsh effects of the pile installation with the aid of FCV-AUT. Also, Mortazavibak et al. [27] studied the bearing capacity of tapered helical piles as a brand-new type of pile using FCV-IUT. In their research, they measured the axial bearing capacity, stiffness, friction, and material efficiency of the proposed model pile.

The geometric scale ratio (λL) in the FCV apparatus can be calculated using the following equation [28]:

$$\lambda_L = \frac{L_m}{\sigma_V / \gamma_S} \quad (1)$$

Where Lm is the length of the model pile, σv is the vertical stress at the bottom of the pile (Installation depth), and γs is the unit weight of the soil sample. The corresponding scale factors for testing model piles in FCV apparatus were provided by Sedran et al. [28], and the scaling factors are provided in Table 1.

Table 1: Scaling factor for model pile testing in FCV

Parameter	Scaling Factor
Length and Displacement	λ_L
Strain	λ_L
Stress	λ_L^2
Force	λ_L^2
Spring Stiffness	λ_L
Elastic Modulus	1

In the present research, the axial bearing capacity of the single-helix and multi-helices piles were evaluated through a comprehensive experimental program. Helical piles, used in this study, consist of steel pipes with one or three welded circular plates to the shaft of the pile with a conical shoe. The model piles were tested in the newly constructed FCV device at Baran Khak va Pey Co, Tehran, Iran, and the capability of the numerical methods to predict the ultimate bearing capacity of piles is evaluated by comparing the experimental and numerical results. To study the effects of the degree of saturation on the ultimate bearing capacity of helical piles, the results of the model piles tested in dry sand are compared with those of model piles tested in saturated sand. Additionally, the effects of installation depth, i.e., scale factor, were evaluated by increasing the uplift pressure in saturated sand conditions.

2. Analytical Bearing Capacity of Helical Piles

The axial bearing capacity of helical piles depends on the failure mechanism of the pile. The failure mechanism of a helical pile is governed by its inter-helix spacing ratio, which is defined as the ratio of the helix spacing to the helix plate diameter (S/Dh).

There are well-known methods for calculating the axial bearing capacity of the helical pile: (1) Individual Bearing Method (IBM), (2) Cylindrical Shear Method (CSM), and (3) Torque Correlated Method. The first two methods are physics-based, while the last one is an empirical method that correlates the installation torque of the helical pile to the ultimate bearing capacity.

The axial bearing capacity of the helical pile is the summation of end bearing capacity and the skin friction of the shaft. The method of calculation of the end bearing capacity largely depends on the helix spacing. The individual bearing failure mechanism typically occurs where the helix spacing is greater than 3Dh, while the cylindrical shear failure mechanism occurs where the helix spacing is less than 1.5Dh[25]. Fig. *1* depicts the two possible failure mechanisms for helical piles.

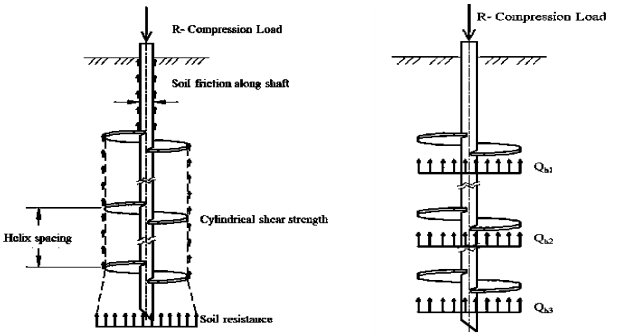

Fig. 1: Pile resisting force in (a) Cylindrical failure mechanism and (b) Individual failure mechanism

Canadian foundation engineering manual (CFEM) provided the formulation for estimating the ultimate capacities of helical piles [29]. The CFEM formulation Can be summarized as follows:

$$R = Q_t + Q_f \tag{2}$$

Where Q_t is the total multi-helix pile capacity, and Q_f is the shaft skin resistance.

$$Q_t = \sum Q_h \tag{3}$$

Where;

$$Q_h = A_h\left(S_u N_c + \gamma D_h N_q + 0.5\gamma B N_\gamma\right) \tag{4}$$

Where:

A_h: Projected helix area

S_u: Undrained shear strength

γ: Unit weights

D_h: Depth to helical plate

B: Diameter of helical plate

N_c, N_q, N_γ: Bearing capacity factor for the local shear condition, presented in Table 10.1 of CFEM.

Q_f is calculated as follows:

$$Q_f = \sum \pi D \Delta l \, f_s \tag{5}$$

Where:

D: Diameter of pile shaft

ΔL: Pile length over which the terms πD and f_s are considered constant

*f*s: sum of friction and adhesion between soil and pile

$$f_s = \sigma_v K \tan\delta \tag{6}$$

In which σ_v is the effective vertical stress at mid-depth of the soil, K = 2(1-sin (ϕ)). δ, and ϕ are the interface friction and frictional resistance angle, respectively.

The analytical method is used to calculate the bearing capacities of piles used in this study. The computed values are then compared with those of the experimental ones.

3. Numerical Modeling

Prior to the fabrication of a new Frustum Confining Vessel capable of simulating the saturated sand conditions, a numerical optimization on the dimensions of the device was carried out. In this regard, reviewing the present FCV apparatuses all around the world, nine sets of dimensions are proposed (Table 2) and examined through finite element modeling in 2D-Axisymmetric modeling space via Abaqus CAE ®.

Table 2: Proposed dimensions

Model	Wall Angle °	Top Diameter mm	Bottom Diameter mm
Model 1	72	400	1050
Model 2	72	500	1150
Model 3	72	600	1250
Model 4	63	400	1420
Model 5	63	500	1520
Model 6	63	600	1620
Model 7	59	400	1600
Model 8	59	500	1700
Model 9	59	600	1800

In order to consider the effects of Soil-Wall interaction on the stress distribution in depth of the device, the contact between the soil and the steel wall is defined using the Penalty method in two tangential and normal directions. For this purpose, normal direction contact is defined as "Hard Contact", while tangential direction contact is defined as a frictional behavior. Different skin friction angles are represented, as demonstrated in Table 3, and the developed models are evaluated in terms of vertical stress gradient in depth at the centerline of the device.

As seen in Figure 2, as the skin friction angle increases, the vertical stress distribution shows a more linear realistic trend in the depth of the FCV apparatus.

Based on the measured properties of Anzali sand, which is used in this study, the internal friction angle varies from 31 to 38 degrees. Therefore, the external surface of the soil and the internal surface of the FCV body can be considered as Fully Contacted.

Table 3: Skin friction angles

Skin Friction Angle δ(°)	Friction Coeff. tan(δ)	Equivalent Internal Friction Angle of Soil φ(°)
20	0.36	29.7
24	0.44	32.5
28	0.53	36
32	0.61	40
Fully Contact	–	-

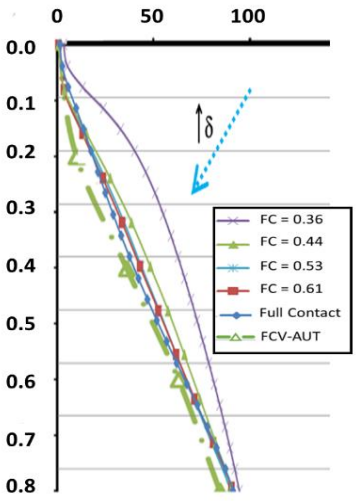

Fig. 2: Vertical stress gradient in depth

In the model, the soil was defined using 4-node, reduced-integration, first-order, axisymmetric solid elements with hourglass control. The model was meshed using quadrilateral elements. Views of the directions of the maximum principle stresses, as well as the stress isosurfaces, are shown in Figure 3.

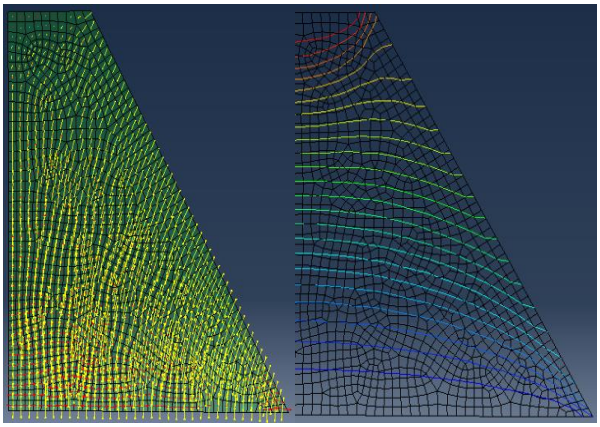

(a) (b)

Fig. 3: (a) Max. Principle Stress and (b) Isosurface Stress plot for new FCV apparatus

Finally, based on the results of numerical simulations, the following dimensions were chosen, and the device was fabricated. More details of the modeling can be found in another paper by the authors, and the readers are encouraged to refer to it [18].

Height (mm)	Top Diameter (mm)	Bottom Diameter (mm)	Wall Inclination Angle (°)
1000	500	1700	31

4. Experimental Work

4.1. Experimental Work Setup

The axial bearing capacity of the helical pile is evaluated in the FCV apparatus. The FCV apparatus, used in this study, FCV-BKP, was constructed at Baran Khak va Pey Co, Tehran, Iran, by the authors. As mentioned in section 3, FCV-BKP has a height of 1000 mm and the top and bottom diameter of 500 mm and 1700 mm, respectively. To grant ease of access during sample preparation, the body of FCV-BKP was divided into two parts by the middle height of the device. To ensure the uniformity of applying the base pressure, a 1700 mm diameter cylinder with a height of 210 mm, equipped with a membrane at its bottom, was added to the FCV-BKP. The bottom pressure is applied by means of applying pressure to the water at the bottom of the apparatus using an air compressor capable of applying up to 600 kPa. The FCV-BKP was equipped with a loading frame used as a support for both the rotary motor drive for pile installation and the hydraulic actuator for applying the axial loads to the model piles during the test. To measure

the precise vertical displacement of the pile head during the experiment, one linear potentiometer with a stroke of 300 mm with a precision of measuring 0.1 mm is mounted to the pile head and the loading frame. To capture the applied load one S-Type load cell with a capacity of 10 tonf was placed between the pile head and the hydraulic actuator's head. In the following, the real and schematic views of the experimental work setup are depicted.

The FCV-BKP apparatus is the first and only FCV apparatus all around the world capable of testing model piles in saturated sand conditions, to the best of the author's knowledge. More details of the construction process of the FCV-BKP apparatus are presented in another research paper by the authors, and readers are encouraged to refer to it for further information [18].

4.2. Model Piles

Helical piles, used in this study, consist of steel pipe with one or three welded circular plates to the shaft of the pile with a conical shoe. In multi-helix piles, helices are spaced apart at a constant ratio, S/D_h=1.5. The model pile dimensions were obtained by scaling down the dimensions of a typical helical pile. The prototype pile has a shaft diameter and helix diameter of 406 mm and 1170 mm, respectively, which are common values in practice. For each test, the dimensions of the model pile were computed based on the scaling law. All the model piles had a length of 750 mm. Figure 4 depicts a layout of the piles used in this study, and Table 4 provides the geometric characteristics of the model piles.

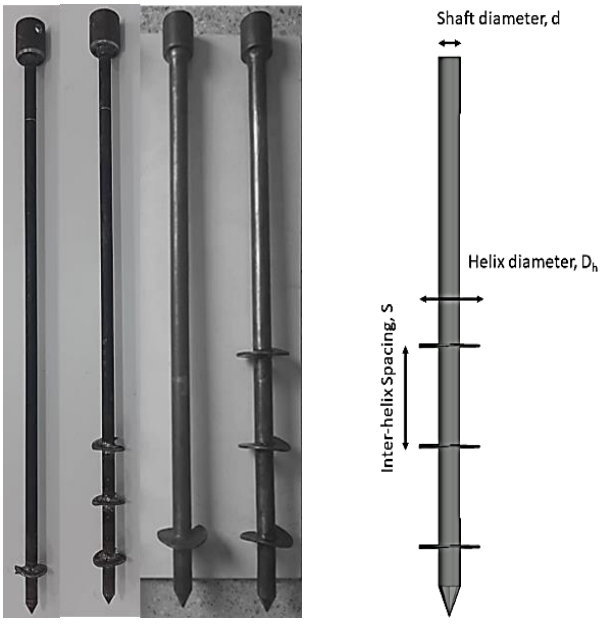

Fig. 4: (a) Layout of helical piles used in this study, (b) Schematic of helical pile

4.3. Installation Process of Piles

Helical pile installation is carried out by applying torque at the end of the pile in the presence of vertical pressure. Figure 5 shows a schematic view of the pile installation procedure. A rotary motor drive mounted on the head piles was used for the installation of helical piles into the sand. The servo-electric rotary drive was fixed on the top of the pile-driving platform, and the pushing force is supplied by the self-weight of the rotary drive, pile, and the upper part of the driving platform. The role of the pile-driving platform is to ensure that the pile is driven to the exact vertical position. The rotary speed of the pile during installation was kept constant at 25 rpm, and the linear speed of pile penetration in the soil sample was about 3-4 mm/sec, which is equal to about 7.2 to 9.6 mm/rev penetration speed.

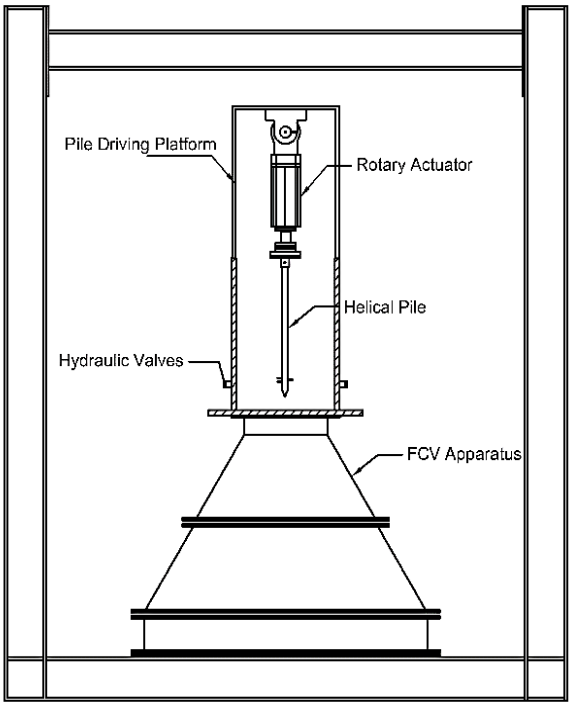

Fig. 5: Schematic view of FCV apparatus during pile installation

4.4. Soil Properties

Interface skin friction between the soil particles and the internal wall of the device plays a key role in generating horizontal and vertical stress distribution in the FCV apparatus. Therefore, the FCV apparatus shall be best suited for simulating the soil-pile interactions in sandy soils, in which the soil strength relies on frictions of the particles rather than the cohesion between them. In this study, the dry sand of Anzali, a coastal city in the north of Iran, was used for sample preparation. According to the Unified Soil Classification System, ASTM D2487 [30], Anzali sand was classified as poorly graded sand (SP).

The specific gravity (Gs) of the solids was measured as 2.69. The mean grain size of the sand (D50), the coefficient of uniformity (CU), and the coefficient of curvature (CC) were found to be 0.215 mm, 1.62, and 0.97, respectively, based on ASTM D6913 [31]. The sand was poured into the apparatus to achieve three relative densities, loose state (Dr ≅ 25%), medium dense state (Dr ≅50%), and dense state (Dr ≅70%). The cohesion and the friction angle of the soil were evaluated through the triaxial consolidated drained test at three different states (Loose, Medium, and Dense) based on the instructions of ASTM D7181[32]. Fig. *6* shows the grain size distribution of Anzali sand. Obtained properties of the used sand are summarized in Table 5.

4.5. Sample Preparation

The internal face of the FCV apparatus was marked at intervals of 50 mm to simplify accurate and homogeneous sample preparation. To overcome the internal friction force of the sand particles during sample preparation, water was added to the sand particles to achieve a moisture content of 4%. For sample preparation, the required weight of sand for each layer was calculated with regard to the under-compaction method; then the sand was poured into the FCV body and compacted to reach the desired surface level. The attained relative densities of sand samples were evaluated using the cylindrical mold with known volume, placed at the centerline of the device at different depths.

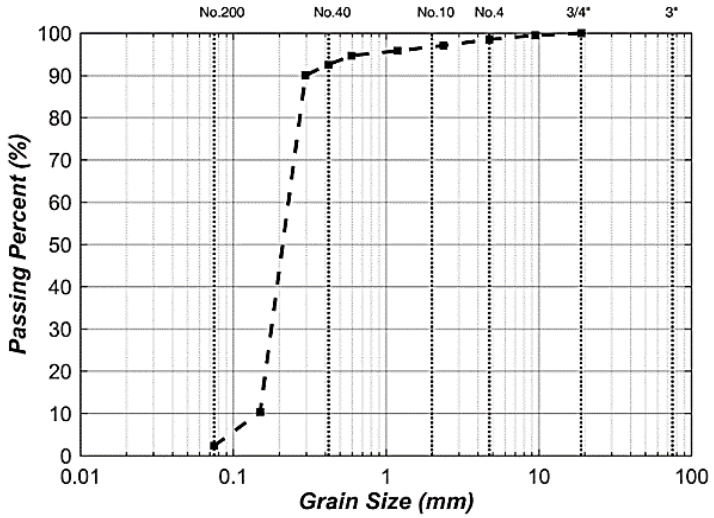

Fig. 6: Grain size distribution for Anzali sand

Table 4: Helical pile dimensions

Pile Type	Scale Factor λ_L	Shaft		Helix			S	H
		Diameter d (mm)	Thickness e (mm)	Diameter D_h (mm)	Thickness e^* (mm)	No. Helix	Spacing	Length (mm)
Prototype 1	1	406	50	1170	50	1	N.A	9750
Prototype 2	1	406	50	1170	50	3	$1.5D_h$	9750
BKP-N01	13	32	4	90	4	1	-	750
BKP-N02	13	32	4	90	4	3	$1.5D_h$	750
BKP-N03	22	32	4	54	4	1	-	750
BKP-N04	22	32	4	54	4	3	$1.5D_h$	750

Results of local relative densities proved the proper sample preparation method. The achieved relative densities have shown a maximum variation of less than 5% (Dr ± 2.5%) between the top and bottom layers.

FCV-BKP provides the capability of testing model piles in saturated conditions. Soil samples within the FCV body are saturated using the flooding method. For this purpose, two valves were installed at the bottom of the FCV-BKP to limit the rate of intake water discharge to the soil sample, as shown in Fig. *7*-c. The rate of water flow was kept constant during the process as low as reasonably practicable, about 0.2 lit/min and less. This is to ensure that the water entering the soil samples would have the least effect on the relative density of soils (Minimum disturbance). The saturation process was stopped when the volume of the water entering the soil sample was equal to or greater than 0.95xVvoid, and the water table level in the FCV apparatus stayed constant at the top of the specimen. The saturation process time varies from 2 to 3 days, based on the relative density of the soil samples.

Table 5: Anzali Soil Properties

Properties	Value
Maximum unit weight, γ_{max} (kN/m^3)	15.46
Minimum unit weight, γ_{min} (kN/m^3)	13.36
Specific gravity, G_s	2.69
Mean grain size, D_{50} (mm)	0.215
Coefficient of uniformity, C_u	1.62
Coefficient of curvature, C_c	0.97
Loose Sand Properties	
Relative density, Dr (%)	25%
Unit weight, γ (kN/m^3)	14.37
Saturated unit weight, γ_{sat} (kN/m^3)	18.43
Internal friction angle, φ	31.0
Medium sand properties	
Relative density, Dr (%)	50%
Unit weight, γ (kN/m^3)	14.90
Saturated unit weight, γ_{sat} (kN/m^3)	18.75
Internal friction angle, φ	36.0
Dense sand properties	
Relative density, Dr (%)	70%
Unit weight, γ (kN/m^3)	15.35
Saturated unit weight, γ_{sat} (kN/m^3)	19.02
Internal friction angle, φ	38.0

4.6. Testing Procedure

Following the sample preparation, the base pressure was applied. The base pressure must be applied gradually in steps to make sure that the relative density of soil samples, especially in loose samples, is not affected. It should be noted that a sudden increase in the amount of applied base pressure may cause liquefaction in saturated sand samples. Therefore, to make sure that the generated excess pore water pressure is completely dissipated during applying the base pressure, the applied load at each step was kept constant for at least 20 minutes in saturated condition tests. After applying the base pressure, the pile was driven into the soil sample using a rotary motor drive.

Then the axial load was applied to the pile end in accordance with the Quick Testing Procedure of ASTM (2013) standard D1143/D1134M 07 [33]. In this method, having in hand an estimate of the ultimate load capacity of the pile, the load is applied in an increment of 5% of the predicted capacity. During each load interval, the load is kept constant for a time interval of not less than 10 minutes for wet conditions and 20 minutes for saturated conditions. During the test, the applied load and the displacement of the head pile are measured and saved at a constant interval time of 1 sec using the Load Cell and Potentiometer, respectively. The test is interrupted when the displacement of the pile head reaches 50% of the helix diameter. At the end, the obtained data are filtered out using zero-phase digital filtering to make them smooth.

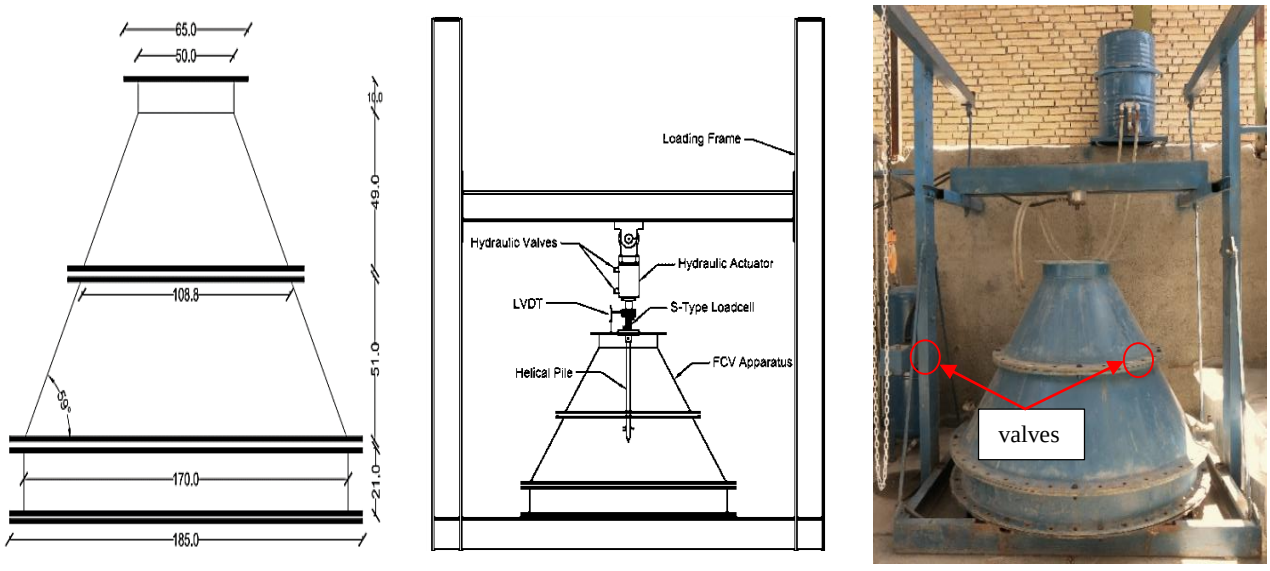

(a) (b) (c)

Fig. 7: (a) Schematic and dimensions of FCV, (b) FCV apparatus during the test, (c) View of the FCV apparatus

4.7. Testing Program

To investigate the axial compressive bearing capacity of helical piles, 18 experimental tests were performed. Tests were categorized into three main classifications; (1) 6 tests in moist sand (W = 4%) with different relative densities, simulating installation depth of 10 to 11 m for pile, (2) 6 tests in saturated soils with different relative

densities, simulating installation depth of 10 to 11 m for pile, and (3) 6 tests in saturated soils, with different relative densities, simulating installation depth of 16.5 to 18.5 m for pile.

In this study, the maximum applied base pressure for moist conditions was chosen to be 200 kPa, which was equal to simulating the installation depth of about 13 m to 14 m at the base of the device. This is the most common real-world depth for installing piles for geotechnical applications. To replicate the same installation depth of 13 m to 14 m at the device base for saturated sand conditions, based on the scale laws, the base pressure was selected to be 121 kPa.

A parametric study with a total number of 18 tests was conducted on helical piles with different helix numbers to study the effects of the number of helices on the axial compressive bearing capacity of piles at different relative densities. The effects of saturation conditions and the effects of the installation depth of piles on the load-displacement behavior are studied as well. Table 6 shows the test descriptions for the current study.

5. Tests Results and Discussion

For different test conditions, the behavior of helical piles can be described using their load-displacement curves. Eighteen tests were performed in FCV-BKP apparatus at different relative densities (Dr, %) and for different helices. The axial bearing capacity of the pile at a certain condition, i.e., specific depth of installation and specific soil condition, is defined as the resisting force corresponding to the displacement of 15% of the helix diameter of the pile.

Table 7 summarizes the axial bearing capacity for tested piles, as well as the numerically predicted bearing capacity using CFEM formulation. The ratio of the predicted to measured load capacities for each test is provided in Table 7 as well. It can be seen that the numerical method provided a close correlation between the measured and numerical predicted results. The ratio of numerically predicted to experimentally measured ultimate bearing capacity is presented in Table 7. The average ratio of analytical to experimental bearing capacity for medium and dense samples is 1.18 with a standard deviation of 0.17, while, for loose sand, the average ratio is 0.61 with a standard deviation of 0.1. In the following sections, the effects of different parameters affecting the bearing compressive capacity of the helical pile, including the relative density of sand, number of helices, saturation condition, and installation depth, are evaluated. Tests were continued to a vertical displacement of half of the helix diameter of piles.

Table 6: Test schedule

	Test No.	Soil Condition	Helix No.	Helix Diameter (mm)	S/D_h	Relative Density (Dr, %)		Uplift Pressure (kPa)	Equivalent simulation depth (m)
State 1	1	moist Condition (Dry Sand with moist, W = 4%)	1	90	N/A	Loose	20-25%	200	13~14
	2					Medium	45-50%		
	3					Dense	65-70%		
	4		3	90	1.5	Loose	20-25%		
	5					Medium	45-50%		
	6					Dense	65-70%		
State 2	7	Saturated Sand	1	90	N/A	Loose	20-25%	121	13~14
	8					Medium	45-50%		
	9					Dense	65-70%		
	10		3	90	1.5	Loose	20-25%		
	11					Medium	45-50%		
	12					Dense	65-70%		
State 3	13	Saturated Sand	1	54	N/A	Loose	20-25%	200	21.6~23.3
	14					Medium	45-50%		
	15					Dense	65-70%		
	16		3	54	1.5	Loose	20-25%		
	17					Medium	45-50%		
	18					Dense	65-70%		

5.1 Effects of Relative Density of Soil

Effects of soil relative density (% Dr) on the bearing capacity of each model pile are shown in Figure 8. As can be seen, for both single-helix and multi-helices piles, the bearing capacity increases more from loose to medium state rather than from medium to dense state. Additionally, it can be seen that soil densification is an

appropriate method for increasing the soil-bearing capacity.

5.2 Effects of Helix Number

To study the effects of helix numbers on the bearing capacity of piles, the load-displacement curves for all three states were plotted and presented in Figures 9 to 11. As illustrated, in State 1, for all relative densities, the load-displacement curve of the one-helix and three-helices piles have shown a similar pattern, especially for Loose and Medium sand. Therefore, the resisting force corresponding to the pile displacement of 15% of the helix diameter is approximately the same. This might be due to the fact that the failure behavior of multi-helices piles with S/Dh = 1.5 is mainly dominated by the cylindrical shear mechanism (CSM). The main discrepancy observed in the behavior of single-helix and three-helices piles is the initial slope of the curves. The initial linear slope for the multi-helices pile is steeper than the slope of the curves for the single-helix pile. The same trend was observed for model piles tested in saturated conditions.

5.3 Effects of Water Content

In the current study, to evaluate the effects of water content on the load-displacement behavior of piles, six tests in saturated conditions were carried out (State 2). In this regard, to make the results comparable, the geometric scale for saturated conditions tests was kept constant. Fig. *12* and Fig. *13* depict the comparison of load-displacement curves of State 1 and State 2 for single-helix and multi-helices piles, respectively. As can be inferred from the figures, the water content in saturated sand (State 2) plays a key role in decreasing the friction between the sand particles, yielding a significant decrease in ultimate bearing capacity and the initial slopes of the load-displacement curves. It is important to mention that besides the lubricant effects of the inter-particle water, with the decrease in the effective stress in depth in the presence of the water, a significant reduction in the bearing capacity of the soil was expected. The ultimate bearing capacity of the piles in saturated sand decreases by 60% on average compared to moist conditions. Additionally, comparing the initial slope of the load-displacement curves in moist and saturated conditions revealed that the soils beneath the helix in moist conditions are mobilized at low displacements such that at a displacement of 5% of the helix diameter, the resisting force is about 70% of the ultimate bearing capacity (corresponding force to displacement of 15% of helix diameter), while, in saturated sand condition, the force corresponded to displacement of 5% of helix diameter is about 30% of the ultimate bearing capacity.

5.4 Effects of Installation Depth of Pile

Effects of the buried depth of piles on their axial bearing capacities, also known as scale effects, were studied by performing six tests in saturated conditions with an increased overburden pressure. In this respect, the uplift pressure at the bottom of the device was chosen to be 200 kPa for saturated tests (State 3), which generates a stress distribution equivalent to stress conditions at a depth of about 23 m on site. It is noteworthy to mention that to make the results of the tests at various installation depths comparable, the obtained values must be converted to their prototype scale. Given that, for each test the forces are multiplied by λ_L^2, and the displacements are multiplied by λ_L (See Table 1). Figure 14 and Figure 15 compare the load-displacement curves for Single-Helix and Multi-Helix piles, respectively, at the prototype scale. The effects of installation depth on the performance of the helical piles can be inferred from the figures. As shown, increasing the installation depth from 10 m to 17.5 m yielded an average increase of about 95%

Table 7: Ultimate bearing capacity of pile

No.	Soil Condition	Helix No.	Helix Dia. (mm)	Relative Density (Dr, %)	Geometric Scale	Axial Bearing Capacity (kN)		Ratio Analytic./ Exp.	Prototype Bearing Capacity (kN)
						Analytical	Experimental		
1	Moist Condition (Dry Sand with moist, W = 4%)	1	90	Loose	13	16.17	20.8	0.78	3 515.2
2				Medium		32.51	34.5	0.94	5 830.5
3				Dense		43.82	37.9	1.16	6 405.1
4		3	90	Loose		16.17	23.5	0.69	3 971.5
5				Medium		32.51	36.1	0.90	6 100.9
6				Dense		43.85	50.0	0.88	8 450.0
7	Saturated Sand	1	90	Loose	13	3.55	7.5	0.47	1 267.5
8				Medium		18.58	14.2	1.31	2 399.8
9				Dense		25.24	18.1	1.39	3 058.9
10		3	90	Loose		3.58	6.3	0.57	1 064.7
11				Medium		18.62	14.9	1.25	2 518.1

12				Dense		25.32	20.2	1.25	3 413.8
13				Loose		2.26	4.00	0.57	2 116.0
14		1	54	Medium		11.28	8.50	1.33	4 496.5
15	Saturated Sand			Dense	23	15.51	12.05	1.29	6 374.5
16				Loose		2.42	4.30	0.56	2 274.7
17		3	54	Medium		11.45	9.60	1.19	5 078.4
18				Dense		15.67	12.15	1.29	6 427.4

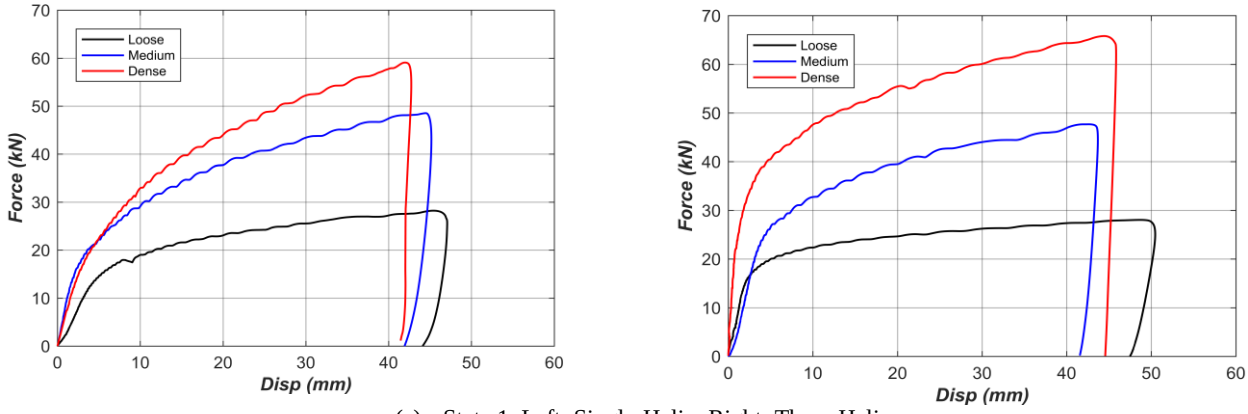

(a) State 1, Left: Single-Helix, Right: Three-Helices

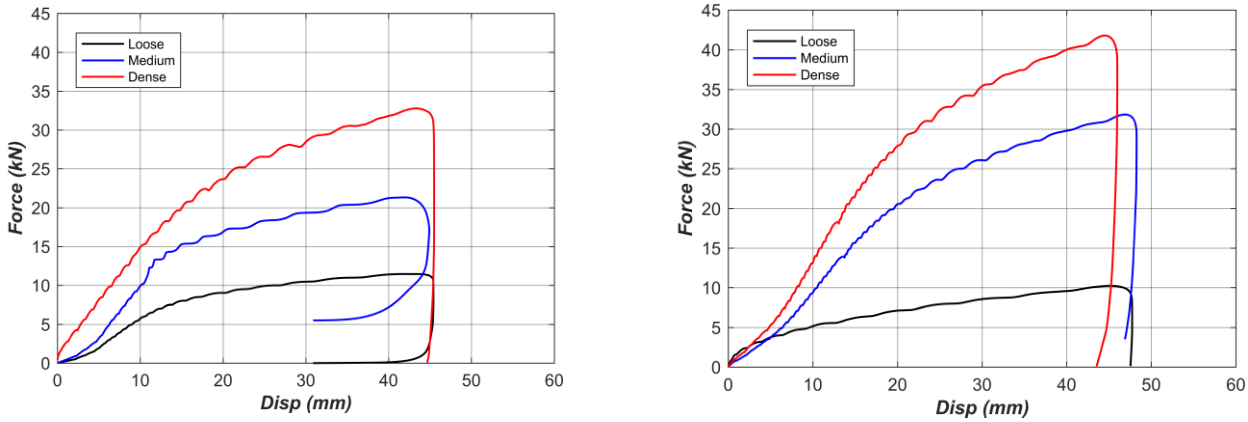

(b) State 2, Left: Single-Helix, Right: Three-Helices

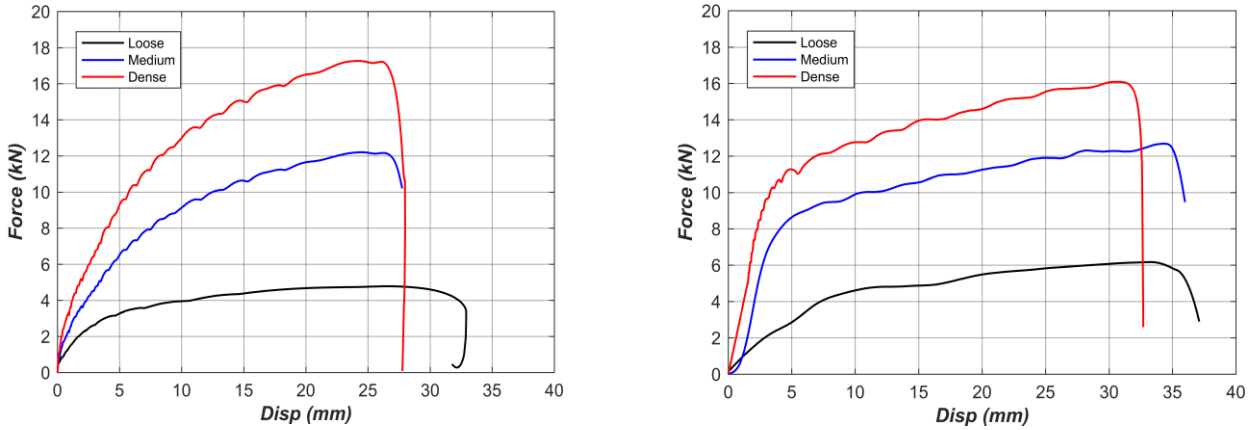

(c) State 3, Left: Single-Helix, Right: Three-Helices

Fig. 8: Effects of relative densities on load-displacement curves

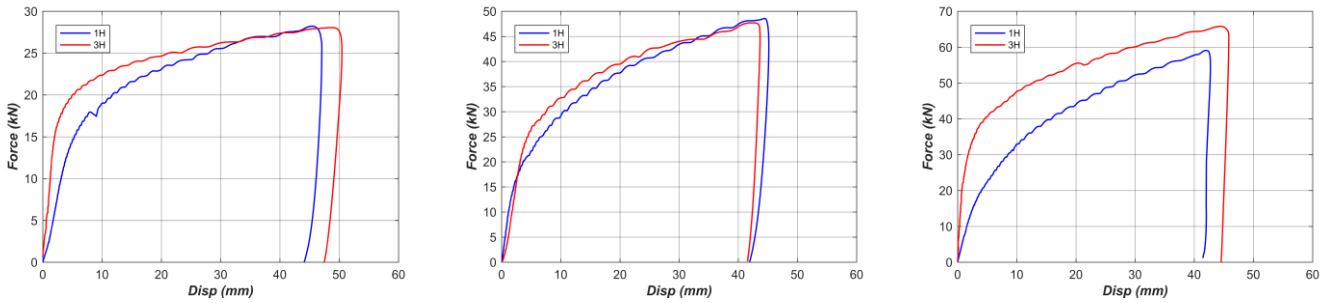

(a) Loose ***(b)*** Medium ***(c)*** Dense

Fig. 9: Load-Displacement curve of the single-helix and multi-helix pile in moist conditions at different relative density

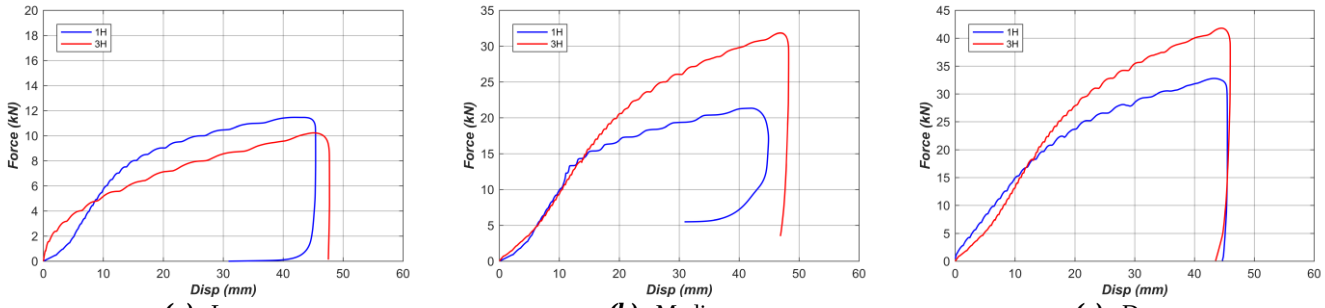

(a) Loose ***(b)*** Medium ***(c)*** Dense

Fig. 10: Load-Displacement curve of the single-helix and multi-helix pile in saturated sand (P=121kPa) at a different relative density

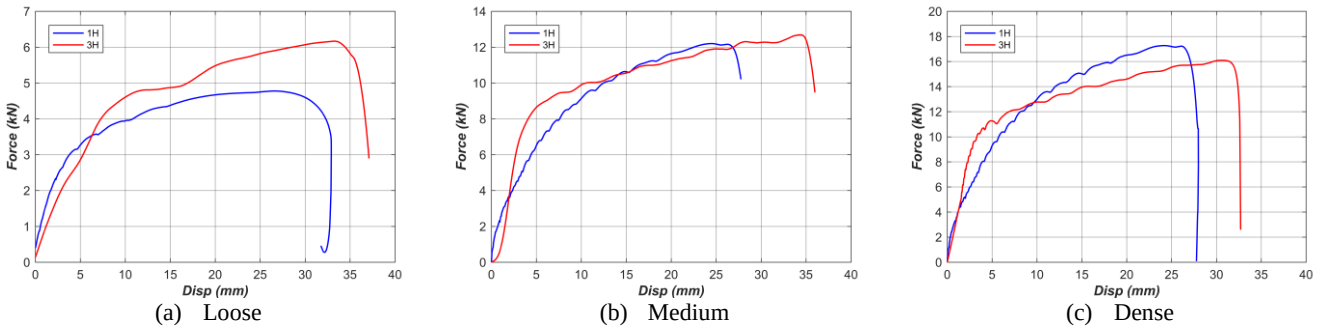

(a) Loose (b) Medium (c) Dense

Fig. 11: Load-Displacement curve of the single-helix and multi-helix pile in saturated sand (P=200kPa) at a different relative density

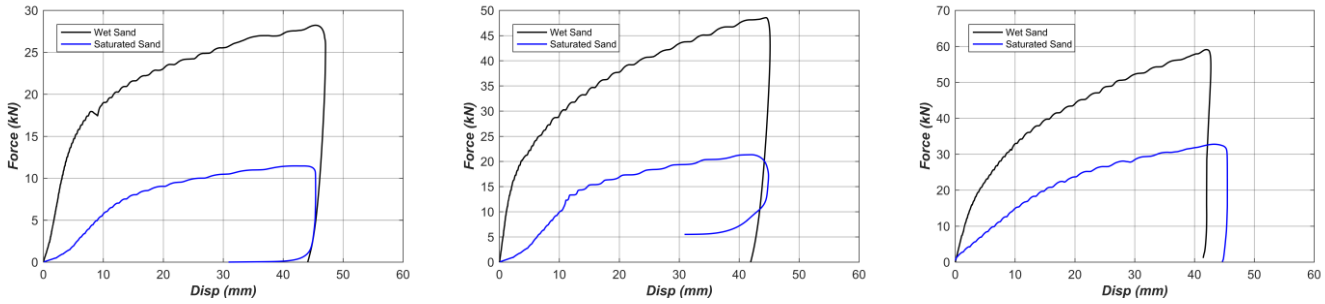

(a) Loose (b) Medium (c) Dense

Fig. 12: Load-Displacement curve of single-helix pile in moist conditions and saturated conditions at a different relative density

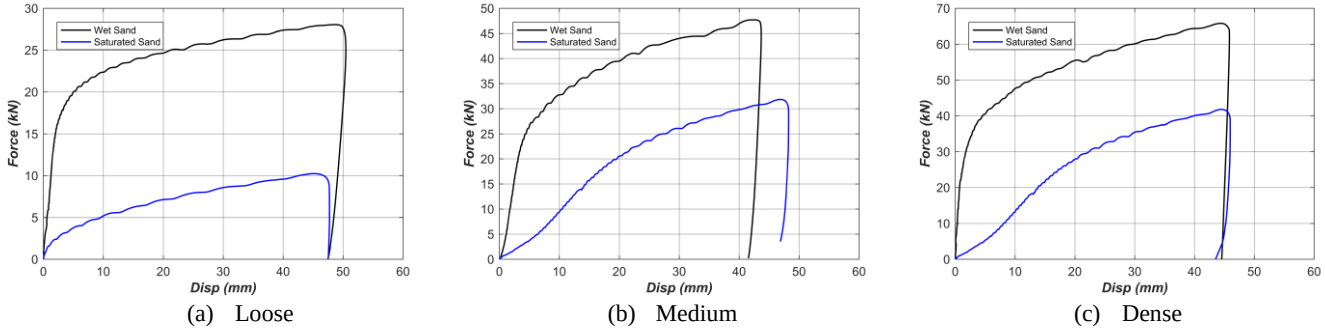

(a) Loose (b) Medium (c) Dense

Fig. 13: Load-Displacement curve of the multi-helix pile in moist conditions and saturated conditions at a different relative density

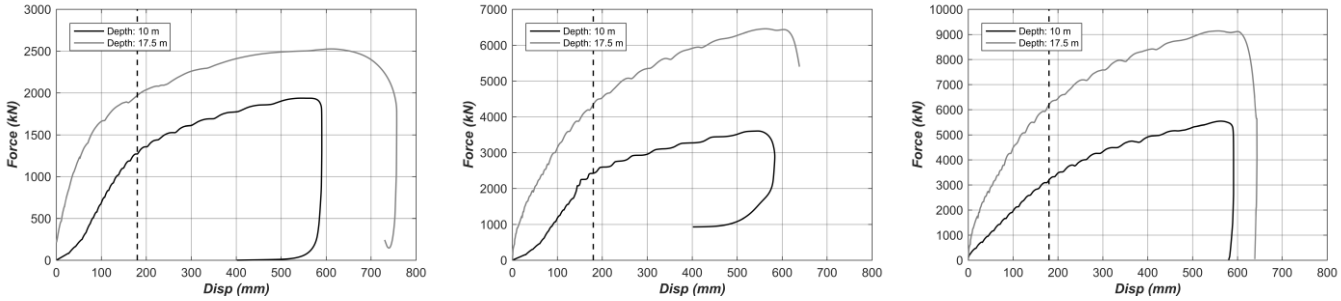

(a) Loose (b) Medium (c) Dense

Fig. 14: Load-Displacement curve of single-helix pile with different installation depths at a different relative density

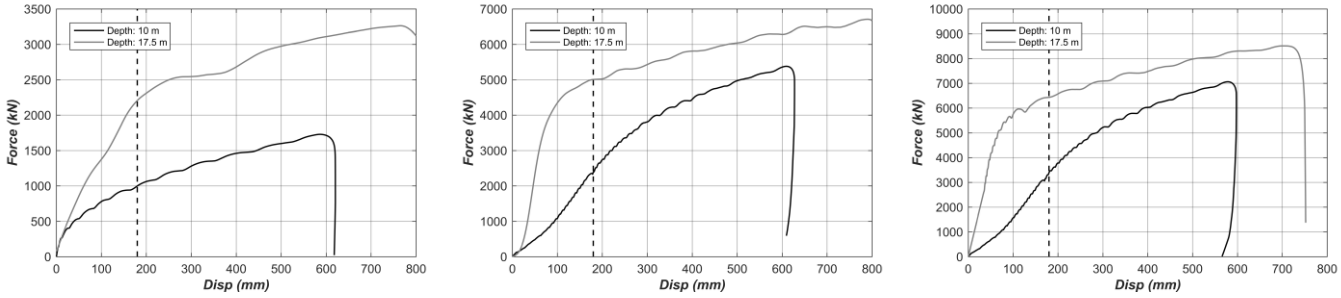

(d) Loose (e) Medium (f) Dense

Fig. 15: Load-Displacement curve of the multi-helix pile with different installation depths at a different relative density

6. Conclusions

An experimental testing program was designed to study the bearing capacity of helical piles. A total of 18 tests were carried out using FCV-BKP, which is, to date, the only FCV apparatus capable of simulating the saturated conditions to the best of the author's knowledge. The study focused on determining the effects of the water content of sands on the load-displacement behavior of helical piles, as well as the effects of the installation depth on the bearing capacity of helical piles. The obtained test results of axial compressive bearing capacity of a single-helix and multi-helices piles in the sand under different relative density conditions are compared. The findings of the experimental study can be summarized as follows:

(1) At a constant helix number, as the relative density increases, the bearing capacity increases, and soil densification can be considered as a potential method for strengthening soil.

(2) In wet sand conditions, the soil beneath the helix is mobilized at low displacements such that at a displacement of 5% of the helix diameter, the resisting force is about 70% of the ultimate bearing capacity (corresponding force to a displacement of 15% of helix diameter). On the other hand, in saturated sand conditions, the force corresponded to a displacement of 5% of helix diameter is about 30% of the ultimate bearing capacity.

(3) The obtained experimental results confirm the predicted failure mechanism for multi-helix piles with the spacing ratio of 1.5. Based on the literature, helical piles with a spacing ratio of 1.5 would be cylindrical shear failures.

(4) Increasing the number of helices at low spacing ratio, $S/D_h < 3$, shows no significant effects on the ultimate bearing capacity of helical piles. The reason for this position is that at a low spacing ratio, the soil beneath each helix cannot be mobilized to resist the applied axial loads individually.

(5) At a constant geometric scale factor, i.e., constant installation depth, increasing the water content has shown a significant effect on the ultimate bearing capacity. On average, the bearing capacity was reduced by 60%. The observation can be justified given the lubricant effects of the excess inter-particle water, as well as the reduced effective stress due to the presence of pore water pressure.

(6) In saturated soil conditions, as the installation depth increased, both in single-helix and multi-helix piles, the ultimate bearing capacity increased.

(7) The average ratio of analytical to experimental bearing capacity for medium and dense relative densities was 1.18 with a standard deviation of 0.17, while for loose sand conditions the average ratio was 0.61 with a standard deviation of 0.1. Totally these values confirm the accuracy of analytical methods. It should be noted that the soil sample preparation for loose sand is more susceptible to disturbance. Therefore, the ratios were calculated separately for loose sand conditions.

(8) By increasing the installation depth in saturated sand conditions, the bearing capacity increases exponentially.

By a 75% increase in the installation depth, the bearing capacity increased by 95%.

Declaration of Competing Interest

The authors declare that they have no known competing financial interests or personal relationships that could have appeared to influence the work reported in this paper.

References

[1] M. Sakr, A. Nazir, W. Azzam, and A. Sallam, "Model study of single pile with wings under uplift loads," *Applied Ocean Research*, vol. 100, 2020.

[2] S. N. Rao, Y. V. S. N. Prasad, and M. D. Shetty, "The Behaviour of Model Screw Piles in Cohesive Soils," *Soils and Foundations*, vol. 31, pp. 35-50, 1991.

[3] L. P. Andina Sprince, "Helical pile behavior and load transfer mechanism," presented at The 10th International Conference, Vilnius, Lithuania, 2010.

[4] A. Eslami and B. H. Fellenius, "Pile capacity by direct CPT and CPTu methods applied to 102 case histories," *Canadian Geotechnical Journal*, vol. 34, p. 19, 1997.

[5] A. M. A. Fateh, A. Eslami, and A. Fahimifar, "A study of the axial load behaviour of helical piles in sand by frustum confining vessel," *International Journal of Physical Modelling in Geotechnics*, vol. 18, pp. 175-190, 2018.

[6] J. Harnish, "Helical pile installation torque and capacity correlations," Masters of Science Electroninc Thesis and Dissertation Repository. 2855, Civil Engineering, University of Western Ontario, 2015.

[7] J. Khazaei and A. Eslami, "Behavior of Helical Piles – as a Geoenvironmental Choice – – by Frustum Confining Vessel," *Advances in Science and Technology Research Journal*, vol. 10, pp. 8-22, 2016.

[8] D. Kim, K. Baek, and K. Park, "Analysis of the Bearing Capacity of Helical Pile with Hexagonal Joints," *Materials (Basel)*, vol. 11, Oct 2 2018.

[9] N. P. Kurian and S. J. Shah, "Studies on the behaviour of screw piles by the finite element method," *Canadian Geotechnical Journal*, vol. 46, pp. 627-638, 2009.

[10] R. S. Merrifield, "Ultimate Uplift Capacity of Multiplate Helical Type Anchors in Clay," *Journal of Geotechnical and Geoenvironmental Engineering*, vol. 137, pp. 704-716, 2011.

[11] A. Mohammadi, T. Ebadi, and M. R. Boroomand, "Physical Modelling of Axial Compressive Bearing Capacity of Instrumented Piles in Oil-Contaminated Sandy Soil," *Iranian Journal of Science and Technology, Transactions of Civil Engineering*, vol. 44, pp. 695-714, 2019.

[12] H. Nagai, T. Tsuchiya, and M. Shimada, "Influence of installation method on performance of screwed pile and evaluation of pulling resistance," *Soils and Foundations*, vol. 58, pp. 355-369, 2018.

[13] M. Zare and A. Eslami, "Study of deep foundation performances by frustum confining vessel (FCV)," *International Journal of Civil Engineering*, vol. 12, pp. 271-280, 2014.

[14] M. Zarrabi and A. Eslami, "Behavior of Piles under Different Installation Effects by Physical Modeling," *International Journal of Geomechanics*, vol. 16, 2016.

[15] D. S. Robert G. Horvath, "Frustum confining vessel for testing model piles," *Canadian Geotechnical Journal*, vol. 33, p. 6, 1996.

[16] A. Eslami, S. Moshfeghi, H. MolaAbasi, and M. M. Eslami, "Geotechnical engineering," in *Piezocone and Cone Penetration Test (CPTu and CPT) Applications in Foundation Engineering*, ed, 2020, pp. 1-23.

[17] H. Mortazavibak, A. Halabian, H. Hashemalhosseini, M. Roshanzamir, A. Jafari, and B. Shabadagh, "Design Optimisation of the Size and Geometry of Frustum Confining Vessel," in *13TH INTERNATIONAL CONFERENCE ON THE MECHANICAL BEHAVIOUR OF MATERIALS*, 2019, p. 298.

[18] A. Jassim;, N. Ganjian;, and A. Eslami, "Design and Fabrication of Frustum Confining Vessel Apparatus for Model Pile Testing in Saturated Soil," *Innovative Infrastructure Solutions*, 2022.

[19] A. h. Karimi and A. Eslami, "Physical modelling for pile performance combined with ground improvement using frustum confining vessel," *International Journal of Physical Modelling in Geotechnics*, vol. 18, 2017.

[20] J. Khazaei and A. Eslami, "Geotechnical behavior of helical piles via physical modeling by Frustum Confining Vessel (FCV)," *International Journal of Geography and Geology*, vol. 5, pp. 167-181, 2016.

[21] A. Karimi, A. Eslami, M. Zarrabi, and J. Khazaei, "Study of pile behavior by improvement of confining soils using frustum confining vessel," *Scientia Iranica*, vol. 24, pp. 1874-1882, 2017.

[22] M. Zarrabi and A. Eslami, "Behavior of piles under different installation effects by physical modeling," *International Journal of Geomechanics*, vol. 16, p. 04016014, 2016.

[23] A. M. A. Fateh, A. Eslami, and A. Fahimifar, "Study of soil disturbance effect on bearing capacity of helical pile by experimental modelling in FCV," *International Journal of Geotechnical Engineering*, vol. 11, pp. 289-301, 2017.

[24] H. A. Perko, *Helical Piles: A practical guide to design and installation*: John Wiley & Sons, 2009.

[25] A. J. Lutenegger, "Behavior of multi-helix screw anchors in sand," in *Proceeding of the 14th Pan-American Conference on Soil Mechanics and Geotechnical Engineering*, Toronto, 2011.

[26] E. Shojaei, A. Eslami, and N. Ganjian, "Self-expanded piles: A new approach to unconventional piles

development," *Marine Georesources & Geotechnology*, vol. 39, 2021.

[27] H. Mortazavibak, A. Halabian, H. Hashemalhosseini, and M. Rowshanzamir, "An investigation on the axial response and material efficiency of tapered helical piles," *Journal of Rock Mechanics and Geotechnical Engineering*, vol. 13, 2021.

[28] G. Sedran, D. F. Stolle, and R. G. Horvath, "An investigation of scaling and dimensional analysis of axially loaded piles," *Canadian geotechnical journal*, vol. 38, pp. 530-541, 2001.

[29] C. G. S. F. Committee, *Canadian foundation engineering manual*: Canadian Geotechnical Society., 2006.

[30] A. D2487, "Standard practice for classification of soils for engineering purposes (unified soil classification system). ASTM International, West Conshohocken, PA, 2017," ed, 2017.

[31] A. D6913, *Standard test methods for particle-size distribution (gradation) of soils using sieve analysis*: ASTM International, 2009.

[32] A. D7181, *Standard Test Method for Consolidated Drained Triaxial Compression Test for Soils*: ASTM International, 2020.

[33] A. D1143/D1143M-07, *Standard Test Method for Piles Under Static Axial Compressive Load*: ASTM International, 2013.